Front. Optoelectron. 2014, 7(1): 20–27
DOI 10.1007/s12200-014-0395-5

REVIEW ARTICLE

Semitransparent organic solar cells

Furong ZHU (✉)

Department of Physics and Institute of Advanced Materials, Hong Kong Baptist University, Hong Kong, China

Abstract The organic solar cell technology has attracted great interests due to its potential of low cost solution process capability. Bulk heterojunction organic solar cells offer a potentially much cheaper alternative way to harness solar energy, and can be made flexible and large area. They can also be made translucent and in different colors. As a result, the inexpensive fabrication process such as solution-process techniques, mechanical flexibility, light weight and visible-light transparency features make organic solar technology attractive for application in new markets, such as smart sensors, power generating window panes, building architecture, greenhouses and outdoor lifestyle, etc. After a brief overview of basics of organic photovoltaics, the enhancement of semitransparent organic solar cells over the two competing performance indices of power conversion efficiency and transmittance will be discussed.

Keywords organic photovoltaic, transparent electrode, optical and optimal design, optical admittance analysis

1 Introduction

The direct conversion of solar energy into electricity by solar cells is considered as one of the lending contenders for renewable energy source and green power production as it generates no detrimental effects to the environment. However, the cost relating to power generation is one of the several challenges the photovoltaic technology facing today. The production of Si-based solar cells is approaching 3 GW/year with billion dollars in worldwide revenue, but this figure is only representing a very small proportion of total energy generated ($<1\%$) in the world [1]. Although, Si-based solar cells are still the dominant technology in the current market, other photovoltaic materials such as gallium arsenides and cadmium tellurides are also penetrating into the photovoltaic market, with a desire to reduce the manufacturing cost as well as improve the cell efficiency [2].

The organic photovoltaic technology has attracted great interests due to its potential of low cost solution process capability. Bulk-heterojunction (BHJ) organic solar cells (OSCs) offer a potentially much cheaper alternative way to harness solar energy, and can be made flexible and large area. They can be also made semitransparent and in different colors in building architecture. Polymeric and organic semiconducting materials have been used for fabricating a variety of optoelectronic devices including organic light-emitting diodes (OLEDs) [3–5], organic thin film transistors [6], organic memory devices [7], organic photodetectors [8] and OSCs [9,10]. In addition to the advantages of being lightweight, cost effective and compatible with flexible substrates, many of these organic and polymeric semiconducting materials possess broad absorption spectra, covering the entire visible spectrum as well as the ultraviolet and infrared spectral regions. The high absorption coefficients ($\sim 10^5$ cm^{-1}) enable the use of thin films to achieve both efficient absorption of the incident light and fast response. The development of OSCs is still in its growing stage, particularly the design and optimization of their structure and the performance. The advantages such as low-cost due to possible solution processing technologies render OSC technology attractive for specialized or cost-sensitive applications. There is an increasing activity in this area, and the prospect for OSCs provides a realistic goal for eventual applications. The development of efficient and stable solar cells constitutes the next major step in this field.

2 Basics of organic photovoltaics

OSCs typically consist of a stack of organic functional layers, e.g., a blend layer of electron donor and electron acceptor materials, sandwiched between a front transparent electrode and a reflective counter electrode. The donor and acceptor can be small molecules, conjugated polymers, or a combination of both, which can be prepared using

Received December 9, 2013; accepted December 24, 2013

E-mail: frzhu@hkbu.edu.hk

sublimation and solution processes. Organic photoactive materials, for example, phthalocyanine (donor) and perylene (acceptor) and its derivatives are examples of small molecular materials that are commonly used for application in OSCs.

When donor and acceptor functional organic semiconducting materials are blended, intimate donor-acceptor nanoscale morphology will be achieved. The energy levels of these materials will be meticulously controlled to facilitate charge transfer between the donor and acceptor at the interfaces of the thin films. Under the illumination, the organic photoactive materials, e.g., conjugated polymers or small molecules forming the electron donor region of OSCs, possess delocalized π electrons that result from carbon p orbital hybridization. These π electrons can be excited by light in or near the visible part of solar spectrum from the highest occupied molecular orbital (HOMO) to the lowest unoccupied molecular orbital (LUMO) and holes on the HOMO of the molecules. As a result of the photo-excitation process, electron-hole pairs (exitons) are generated. The energy bandgap between LUMO and HOMO orbitals determines the absorption of light entering to the OSCs.

The performance of OSCs is determined primarily by the following factors: 1) absorption efficiency of the materials for generating photo-induced excitons; 2) the exciton diffusion length; 3) the ratio of the exciton dissociation at the donor/acceptor interface; and 4) the charge collection efficiency at the interfaces of anode/organic and organic/cathode. It has been recognized that the most efficient exciton dissociation in organic materials can occur at donor/acceptor interface [11,12]. Depending on the alignment of energy levels of the donor and acceptor, the dissociation of bound exciton can become energically favorable at the interface. The time scale for such a dissociation is of a few hundred femtoseconds, which is much shorter than any other competing process, thus the exciton dissociation (or charge transfer from the donor to the acceptor) efficiency could also be about 100%. Therefore, the device efficiency will be mainly determined by the remaining two factors: exciton diffusion to donor/acceptor interface and free charge transport to the opposite electrode. It has been reported that the exciton diffusion efficiency can be enhanced by establishing an intimate contact between the donor and acceptor by blending [11] and laminating [12] or co-depositing them [13,14]. Thus controlling the film morphology to form percolating paths to enhance the exciton diffusion, charge transport and charge collection efficiency at anode/organic and organic/cathode interface will be a key for achieving high efficiency OSCs [15].

The primary photo-generated excitations in organic materials do not directly and quantitatively lead to free charge carriers but to form coulombically bound electron-hole pairs, or known as excitons. The binding energy of photo-generated excitons in organic materials, in a range of 200–500 meV [16,17], is about 10 times larger than the ones in conventional inorganic semiconductors, e.g., Si, where photo-excitations typically lead to free carriers directly at room temperature. It is estimated that only 10% of the photo-generated excitons will lead to free charge carriers in pure conjugated polymers [18]. Therefore, a strong electric field is required to break the excitons in organic semiconducting materials. To have an efficient dissociation of excitons, localized electric field can be supplied via externally applied electrical fields or at donor/acceptor interface. At the interface, a strong electric field exists due to the presence of an abrupt potential energy difference at the donor/acceptor interface. Photo-induced charge transfer can occur if excitons reach such interface within their lifetime. The diffusion length of excitons in organic materials is an important parameter to be considered as it not only limits the thickness of a bilayer (donor-acceptor heterojunction configuration), it also affects the power conversion efficiency (PCE) of the whole device. BHJ is widely adopted for application in OSCs. The exciton diffusion length should be of the same order of magnitude as the donor-acceptor phase separation length. Otherwise, excitons decay via radiative or non-radiative path ways before reaching the donor/acceptor interface. The diffusion length of photo-excited excitons in organic photoactive materials is typically in the order of 10–20 nm.

It is known that fullerene and its derivatives are strong electron acceptors. The excitons can be dissociated effectively to form free carriers at donor/fullerene interface. Ultrafast photo-physics studies revealed that the photo-induced charge transfer in such blends occurs in a time scale of 45 fs. This is much faster than other relaxation processes such as photoluminescence (usually occurs at around 1 ns) [19]. The reverse electron transfer from fullerenes back to the polymer is extremely slow. Thus, the quantum efficiency of this dissociation process is close to 100% at the polymer-fullerene interface. However, the separated charges in such blends are metastable at low temperatures. They should be transferred away from the interface before being recombined.

Photo-generated charges in OSCs should be transported effectively toward the respective electrodes within their lifetime. These charge carriers are unable to travel independently unless a driving force is applied. A chemical potential gradient in electrons and holes is built up at the donor/acceptor interface. This potential gradient is generally defined by the difference between the HOMO of the donor and LUMO of the acceptor. This internal electric field correlates closely with the open circuit voltage (V_{oc}) of OSCs and contributes to a field-induced drift of the charge carriers. To enhance the charge transport, asymmetrical contacts are used, e.g., a cathode with a low work function for electron collection and an anode with a high work function for hole collection, to generate an external field in short circuit conditions according to a metal-

insulator-metal configuration. To optimize the PCE and lifetime of OSCs, it is important to understand the charge transport properties under various operation conditions and to identify the loss (or degradation) mechanisms. The complexity of physics operating in OSCs offers a major driving force for new developments. In particular, the correlation between the charge transport/recombination and the device performance parameters (lifetime, efficiency) are not clearly understood and there are no known systematic reports on this topic. The better understanding on charge trapping behavior with respect to the quality of the materials and the process conditions is important for achieving high performance OSCs.

In parallel to the new materials development, detailed understanding of the charge or energy transfer processes and photo-generated exciton dynamics in OSCs is another important knowledge for developing high performance BHJ OSCs. Steady-state photo-induced absorption (PA) using pump-probe technique has been used to study these excited states in the polymer film [20]. The PA and stimulated emission related to singlet/triplet exciton, polaron and bipolarons in pristine polymer films and solutions have been extensively studied [21–24]. The exciton dynamics in OSCs have been focused to better understand the relaxation processes and dynamics of charge separation (from exciton) to weakly bound charge transfer (CT) state (i.e., CT exciton) at the donor-acceptor interface, and its subsequent dissociation to free charge carriers [25–30]. For investigation of relaxation dynamics, one uses time-resolved and transient PA techniques. Detailed transient PA measurements have been carried out in the donor/acceptor blends to give a better understanding of the photo-generated carrier recombination dynamics in OSCs [25,26,29–31]. The results show that charge separation and recombination dynamics in polymer/fullerene interface are very complex with relaxation time scale from femtosecond to nanosecond and microsecond time scale [25]. PA experiment also indicates that significant amount of CT excitons were recombined at the donor/acceptor interface before they have a chance to completely separate forming mobile carriers [25,28]. Various processes such as thermal annealing [27] or new synthesis routes [32] can alter the morphology of the bulk heterojunction mixture and consequently the relaxation dynamics and free carrier yields. For example, using thermal annealing, transient PA demonstrated slower decay and large PA signal from charge carriers [27]. The increase in the yield of dissociated charges by thermal annealing helps to produce solar cell with significantly high efficiency. Thus steady and transient PA is a very powerful tool to investigate the separation, relaxation and recombination dynamics of the photo-generated excitons.

Light absorption in OSCs is limited due to the presence of a mismatch between optical absorption length and the low charge mobility in organic semiconductors. One of the effective ways to improve the performance of OSCs is to use tandem structure, having two or multiple cells vertically stacked in series. This enables each sub-cell to respond actively to different parts of the incident solar radiation. It is important that the thickness of active organic layers or polymer blends in each thin solar cell is optimized to achieve current matching conditions. The tandem structure requires a front sub-cell to be sufficiently transparent to light that is not absorbed. Therefore light can pass through the front semitransparent OSC and is absorbed by the next sub-cell. In addition to the development of high performance tandem OSCs, this paper will focus on the possible designs to realize absorption enhancement in semitransparent organic solar cells over the two competing performance indexes of power conversion efficiency and visible-light transparency.

3 Optical admittance analysis

A conventional OSC consists of a front transparent anode, a stack of photoactive organic layers or blends material that absorbs photons and converts them into electrons and holes, and a reflective cathode. An OSC with a thin film configuration can be considered generally as a multilayer thin film system composed of materials with different optoelectronic properties. For example, OSC of the type: glass/indium tin oxide (ITO)/organic photoactive layer/cathode and the corresponding energy diagram of the functional materials used in the device. Let's assume an organic solar cells has m layers, the effective optical admittance, y_{eff}, of this multilayer system can be defined as $y_{\text{eff}} = C/B$, where B and C can be determined by solving the following characteristic matrix equation [33]:

$$\begin{pmatrix} B \\ C \end{pmatrix} = \left[\prod_{j=1}^{m} \begin{pmatrix} \cos\delta_j & (\mathrm{i}\sin\delta_j)/y_j \\ \mathrm{i}y_j\sin\delta_j & \cos\delta_j \end{pmatrix} \right] \begin{pmatrix} I \\ y_{m+1} \end{pmatrix}, \quad (1)$$

where y_j and y_{m+1} are the optical admittance of the jth layer and substrate respectively. I is the unit matrix, δ_j is the angular phase given by

$$\delta_j = \frac{2\pi N_j d_j \cos\theta}{\lambda}, \quad (2)$$

where d_j is the actual thickness of the jth layer in this m layered structure, and N_j is the corresponding complex refractive index given by $N_j = n_j(\lambda) - \mathrm{i}k_j(\lambda)$, where $n_j(\lambda)$ and $k_j(\lambda)$ are real and imaginary parts of N_j, respectively. The characteristic matrix Eq. (1) takes into account the effect of the multiple reflections in a multi-layer structure. Using the value y_{eff} calculated from an m layered thin film system, the total reflectance as a function of wavelength, $R(\lambda)$, can be expressed as

$$R(\lambda) = \left| \frac{N_0 - y_{\text{eff}}}{N_0 + y_{\text{eff}}} \right|^2, \quad (3)$$

where N_0 is the refractive index of air. The reflectance thus obtained depends on the wavelength of the incident radiation. Assuming normal incidence, the total transmittance as a function of wavelength, $T(\lambda)$, can be expressed as

$$T(\lambda) = [1-R(\lambda)]\prod_{j=1}^{m}\psi_j, \tag{4}$$

where ψ_j is the ratio of the time averaged numerical magnitude of the Poynting's vector at the jth and $(j-1)$th boundaries, and is given by

$$\psi_j = \frac{\mathrm{Re}(Y_{j+1})}{\mathrm{Re}(Y_j)\left|\cos\delta_j + Y_{j+1}\sin\delta_j/N_j\right|^2}, \tag{5}$$

where $\mathrm{Re}(Y_{j+1})$ and $\mathrm{Re}(Y_j)$ represent the real parts of the effective admittance for the $(j+1)$th, Y_{j+1}, and jth, Y_j, layers respectively. The total absorbance as a function of wavelength, $A(\lambda)$, in this m layer system can be calculated from the following expression:

$$A(\lambda) = 1-T(\lambda)-R(\lambda). \tag{6}$$

Similarly, the net absorbance of the ith layer, $A_i(\lambda)$, in an m layer organic solar cell can be determined by

$$A_i(\lambda) = [1-R(\lambda)][1-\psi_i(\lambda)]\prod_{j=1}^{i-1}\psi_j(\lambda). \tag{7}$$

Using the flux of the incident solar radiation $F(\lambda)$, measured in $\mathrm{W\cdot m^{-2}\cdot \mu m^{-1}}$, for example AM1.5G spectrum, the integrated absorbance of any individual layer, $\overline{A}_i$, and the total absorbance of an m-layered system, e.g., an OSC, $\overline{A}$ can be calculated as

$$\overline{A}_i = \frac{\int A_i(\lambda)F(\lambda)\mathrm{d}\lambda}{\int F(\lambda)\mathrm{d}\lambda}, \tag{8}$$

$$\overline{A} = \frac{\int A(\lambda)F(\lambda)\mathrm{d}\lambda}{\int F(\lambda)\mathrm{d}\lambda}. \tag{9}$$

Similarly, the total reflectance, $\overline{R}$, and total transmittance, $\overline{T}$, of an OSC under AM1.5G spectrum can be expressed and calculated as

$$\overline{R} = \frac{\int R(\lambda)F(\lambda)\mathrm{d}\lambda}{\int F(\lambda)\mathrm{d}\lambda}, \tag{10}$$

$$\overline{T} = \frac{\int T(\lambda)F(\lambda)\mathrm{d}\lambda}{\int F(\lambda)\mathrm{d}\lambda}. \tag{11}$$

Thus it is possible to calculate absorbance, transmittance and reflectance of an entire device and also an active region in an OSC. The optical performance of organic solar cells can then be analyzed and optimized based on the above principles discussed. Optical admittance analysis can be employed to investigate light distribution and absorption enhancement in a semitransparent OSC, realizing simultaneous optimization of cell performance and visible-light transparency.

4 Optical enhancement in semitransparent organic solar cells

We now discuss simultaneous optimization of the cell performance and the visible-light transparency of semitransparent OSCs, for example, with a cell configuration of glass/ITO/poly (styrene sulfonate)-doped poly (3, 4-ethylene dioxythiophene) (PEDOT:PSS)/polymer blend/interlayer/upper ITO cathode. The upper cathode in semitransparent OSCs is much more demanding, serving as a charge collecting contact and a transparent conducting capping electrode to overcome the lateral current limitation. The thickness of upper ITO electrode can be optimized to enhance the visible-light transparency of semitransparent OSCs. The integrated absorptance, $\overline{A}$, of photoactive layer calculated using Eq. (9), and the integrated total transmittance, $\overline{T}$ calculated using Eq. (11), of the semitransparent OSCs can be analyzed and optimized prior to the device fabrication. The optimal device structure can be obtained by maximizing light absorption in the active layer, e.g., a blend of region regular poly(3-hexylthiophene)(P3HT):[6,6]-phenyl-C61-butyric acid methyl ester (PCBM), and the transmission of the semitransparent OSCs. This simulation uses the dispersive refractive index and extinction coefficient of the materials that measured from the ellipsometry. In this work, an ultrathin Ca/Ag interlayer was used. It is observed that the semitransparent OSC with an upper cathode combination of Ca (10 nm)/Ag (10 nm)/ITO is superior to a thin transparent metal cathode. A semitransparent OSC with only a bilayer metal cathode, e.g., Ca (10 nm)/Ag (10–15 nm), causes a large internal reflection at the metal/air interface due to its high refractive index. The upper ITO cathode serves as a transparent conducting index matching layer to enhance the total light transmission in semitransparent OSCs. In addition, the upper ITO contact also acts as a passivation layer to protect the underlying functional organic layers in semitransparent OSCs from any possible moisture attack from the environment.

The integrated absorbance and the total transmittance as a function of P3HT: PCBM layer thickness for semitransparent OSCs of the type: glass/ITO/P3HT:PCBM (25–300 nm)/Ca (10 nm)/Ag (10 nm)/upper-ITO-electrode, were calculated. The integrated transmittance and absorptance of the semitransparent OSCs as a function of the

P3HT:PCBM active layer thickness is shown in Fig. 1. In the device application, a thin silver layer is used to improve the lateral electrode conductivity and also prevents the possible damage to the underlying calcium and polymer blend during the ITO deposition. It shows that the transmittance of a semitransparent OSC decreases from about 50% to 25% when the thickness of the P3HT:PCBM layer increases from 25 to 300 nm. According to the simulation results shown in Fig. 1(a), a 75 nm thick active layer of P3HT:PCBM for a semitransparent OSC is chosen. This is because a thinner OSC, e.g., a relative maximum light absorption occurred at a 75 nm P3HT:PCBM layer enables to achieve good charge transport properties and also possesses a reasonable visible-light transparency. For example, a semitransparent OSC having an integrated absorptance of 34% in the P3HT:PCBM layer possesses a visible-light transparency of 42%, as shown in Fig. 1(a). A photo picture taken for a semitransparent OSC having an optimized device structure of glass/ITO/PEDOT:PSS (40 nm)/P3HT:PCBM (75 nm)/Ca (10 nm)/Ag (10 nm)/ITO (60 nm) is shown in Fig. 1(b).

In practical application, a semitransparent OSC with an optimized interlayer/ITO cathode can be more preferred than a layer of a thin transparent metal cathode. A semitransparent OSC finished with a thin metal cathode, e.g., Ca (10 nm)/Ag (10–15 nm), causes a large internal reflection at the metal/air interface due to its high refractive index. When an upper cathode of Ca (10 nm)/Ag (10 nm)/ITO is used, the unique electric and optical properties of ITO capping layer enable it functions as a transparent conducting index matching layer to enhance the total light transmission. This aside, ITO layer also acts as an upper passivation layer to protect the OSCs.

The effect of upper ITO electrode thickness on the total transmittance and integrated absorbance of P3HT:PCBM layer in the semitransparent OSCs is analyzed. The calculated results are plotted in Fig. 2. For a semitransparent OSC with a configuration of glass/ITO/PEDOT:PSS (40 nm)/P3HT:PCBM (75 nm)/Ca (10 nm)/Ag (10 nm)/upper-ITO, the results indicate that a maximum transmittance of the semitransparent OSCs can be achieved at an upper ITO cathode thickness of 50 nm, whereas the maximum light absorption is occurred in P3HT:PCBM (75 nm) at an upper ITO cathode thickness of 80 nm. To illustrate the point clearly, a gray region is depicted in Fig. 2, which corresponds to an ITO layer thickness chosen in the region that could result in an OSC achieving possible maximum light absorption and transmission simultaneously. As a result, a 60 nm thick upper ITO is selected for OSCs with a configuration of glass/ITO/PEDOT:PSS (40 nm)/P3HT:PCBM (75 nm)/Ca (10 nm)/Ag (10 nm)/ITO (60 nm). This leads to a total transmittance 42% and an integrated absorbance of 34% for the resulting semitransparent OSCs.

The wavelength dependent transmittance, $T(\lambda)$, of the semitransparent OSCs with two different cathode structures of Ca (10 nm)/Ag (10 nm) and Ca (10 nm)/Ag (10 nm)/ITO (60 nm) was also calculated. The simulated and measured $T(\lambda)$ of semitransparent OSCs made with two different cathode structures of Ca (10 nm)/Ag (10 nm) and Ca (10 nm)/Ag (10 nm)/ITO (60 nm) are shown in Fig. 3 (a). It can be seen clearly that semitransparent OSCs with an upper transparent cathode of Ca (10 nm)/Ag (10 nm)/ITO (60 nm) possess a higher $T(\lambda)$ throughout the whole visible light wavelength region as compared to a structurally identical semitransparent OSC having a thin layer Ca (10 nm)/Ag (10 nm) cathode. The Ca (10 nm)/Ag (10 nm) cathode in semitransparent OSC causes a large amount of internal reflection at the metal/air interface, leading to a low $T(\lambda)$. The visible-light transparency of the

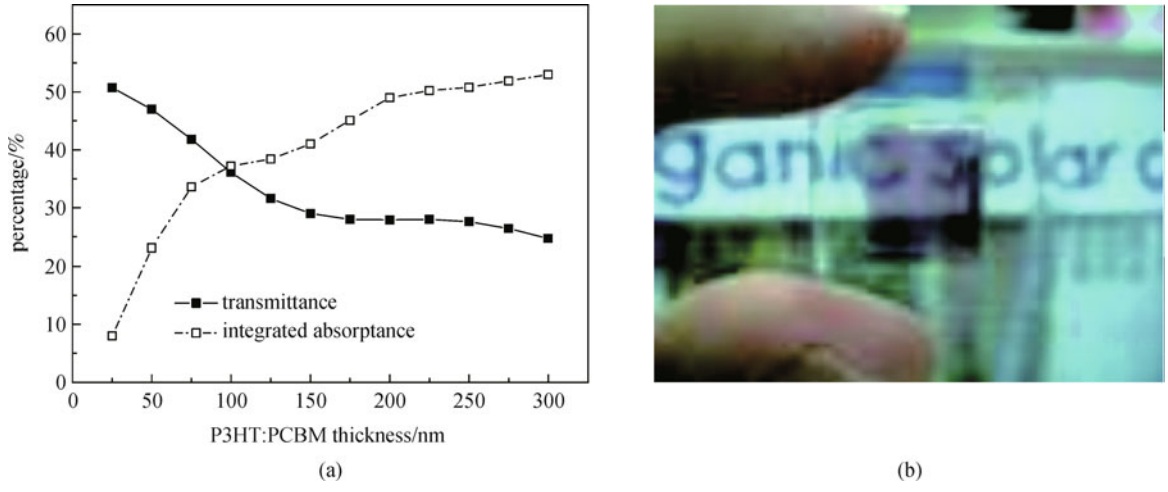

Fig. 1 (a) Calculated transmittance and integrated absorptance of P3HT:PCBM active layer as a function of its layer thickness for semitransparent OSCs of the type: glass/ITO/PEDOT:PSS (40 nm)/P3HT:PCBM (25–300 nm)/Ca (10 nm)/Ag (10 nm)/ ITO (60 nm); (b) a photo picture showing a semitransparent OSC having an optimized cell structure of glass/ITO/PEDOT:PSS (40 nm)/P3HT:PCBM (75 nm)/Ca (10 nm)/Ag (10 nm)/ITO (60 nm)

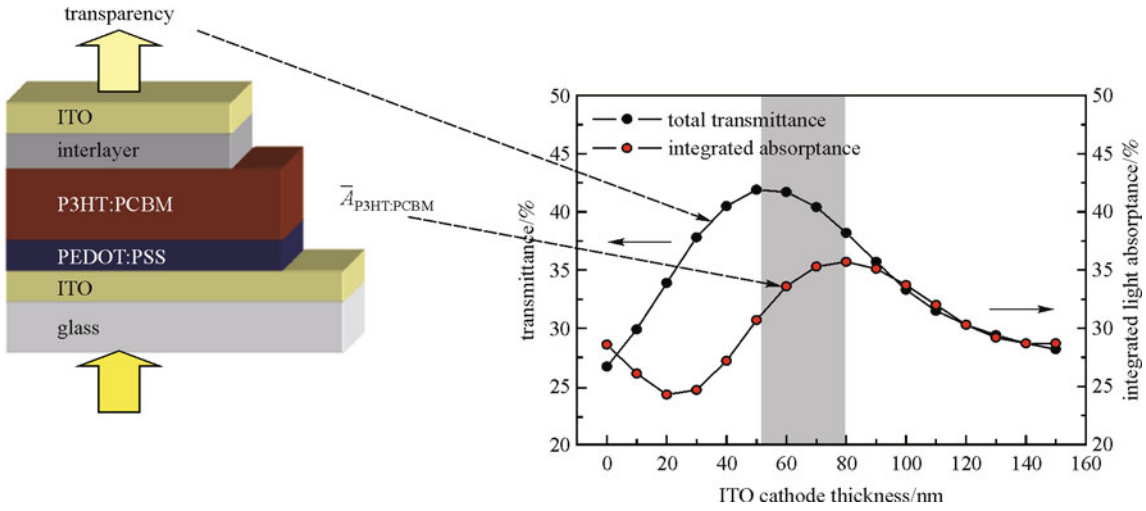

Fig. 2 Calculated results showing the effect of the upper ITO layer thickness on the integrated absorbance of P3HT:PCBM layer and the transmittance of a semitransparent OSC of the type: glass/ITO/PEDOT:PSS (40 nm)/P3HT:PCBM (75 nm)/Ca (10 nm)/Ag (10 nm)/ITO (0–60 nm)

semitransparent OSCs with an upper ITO capping layer, e.g., simulated (solid black line) and measured (solid red line) in Fig. 3(a), is higher than that of the semitransparent OSC having an upper Ca (10 nm)/Ag (10 nm) cathode, e.g., simulated $T(\lambda)$ in Fig. 3(a). The measured $T(\lambda)$ of the semitransparent OSCs having ITO capping layer does not overlap exactly as compared to that of the simulated $T(\lambda)$ obtained for the same device, the deviation in the $T(\lambda)$ between the experimental and calculated transparency in the semitransparent OSCs may be attributed to the assumption of a perfect film smoothness, while the non-homogeneity of the organic thin films may be possible in the actual OSCs. From the above discussion, it is clear that the structure and the process optimization of ITO-based cathode are very important for the design and fabrication of high performance semitransparent OSCs. Simultaneous optimization of cell performance and visible-light transparency for a semitransparent OSC can be realized.

Based on the knowledge gained on the improved upper transparent cathode and emerging cell design concepts, semitransparent OSCs with different upper cathode contacts were fabricated and characterized. The performance of a control OSC with the configuration of glass/ITO/PEDOT:PSS (40 nm)/P3HT:PCBM (75 nm)/Ca (10 nm)/Ag (100 nm) was also analyzed for comparison studies. The photo-current density – voltage ($J-V$) characteristics measured for a control OSC and two structurally identical semitransparent OSCs with different upper transparent cathodes of Ca (10 nm)/Ag (10 nm) and Ca (10 nm)/Ag (10 nm)/ITO (60 nm) were measured using a calibrated AM1.5 solar simulator in the nitrogen glove box. The results are plotted in Fig. 3(b).

According to the $J-V$ characteristics, as shown in Fig. 3 (b), the control OSC yield a higher short circuit current density (J_{sc}) of 8.22 mA/cm^2 in comparison with that of the semitransparent OSCs with Ca (10 nm)/Ag (10 nm) cathode (J_{sc}: 5.20 mA/cm^2) and Ca (10 nm)/Ag (10 nm)/ITO (60 nm) (J_{sc}: 6.89 mA/cm^2). It is shown that the fill factor of a semitransparent OSC with a cathode of Ca (10 nm)/Ag (10 nm) is lower than that of a semitransparent OSC having an upper Ca (10 nm)/Ag (10 nm)/ITO (60 nm) transparent cathode and a control OSCs, which limits the energy conversion efficiency. The increase in the photo-current density of the semitransparent OSC with a cathode of Ca (10 nm)/Ag (10 nm) in the forward bias region is slightly lower than that measured for semitransparent OSC with a Ca (10 nm)/Ag (10 nm)/ITO (60 nm) cathode and the control OSC. This implies that the semitransparent OSC with only a thin metal cathode has a higher series resistance than the one having a Ca (10 nm)/Ag (10 nm)/ITO (60 nm) upper cathode. It is clear that semitransparent OSCs with a Ca (10 nm)/Ag (10 nm)/ITO (60 nm) cathode also possesses a high V_{oc} as compared to the semitransparent OSC with a thin metal cathode. The decrease in V_{oc} observed in semitransparent OSCs without upper ITO capping layer could be attributed to the poor contact at organic/Ca/Ag interface, as a total 20 nm thick Ca/Ag stack formed on the polymer blend is likely discontinuous.

The development of semitransparent OSCs is still in its early stage, particularly the design and optimization of cell structure and the device performance. The semitransparent OSC technology can be advanced through new materials development, especially new organic photoactive materials with enhanced absorption in near infrared (NIR) region and high performance transparent electrodes. Unlike conventional solar cells that absorb visible and infrared light to generate power, a semitransparent OSC with NIR absorber allows visible light to pass through it while

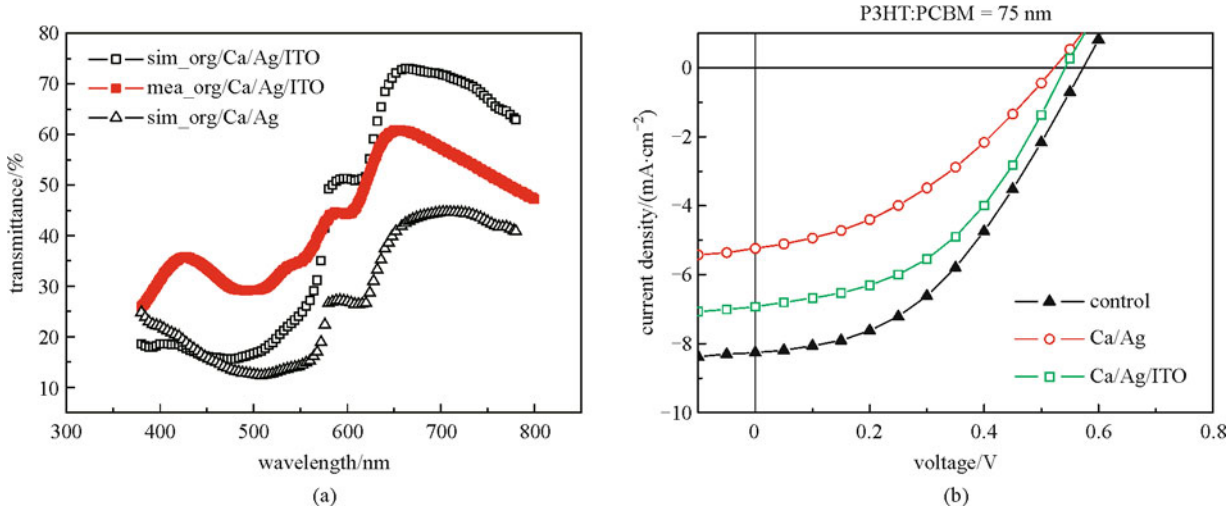

Fig. 3 (a) Transmission spectra calculated for two structurally identical semitransparent OSCs with Ca (10 nm)/Ag (10 nm) and Ca (10 nm)/Ag (10 nm)/ITO (60 nm) upper cathodes, respectively. The red symbols represented the transmission spectral measured for semitransparent OSCs made with a Ca (10 nm)/Ag (10 nm)/ITO (60 nm); (b) comparison of J–V characteristics measured for a control OSC, semitransparent OSCs with upper cathodes of Ca (10 nm)/Ag (10 nm) and Ca (10 nm)/Ag (10 nm)/ITO (60 nm)

absorbs UV and NIR radiation and converts it into electricity. In the near future, a low-cost, semitransparent OSC technology will be eventually proven viable that can be integrated onto window panes in homes, offices, and even automobiles, enhancing the functionality of already utilized transparent surfaces. The additive semitransparent OSC technology enables to modify the glass transparency, but the non-transmitted light would be utilized for power generation.

5 Conclusions

Substantial progress has been made in OSCs by emergence of new organic photoactive materials with tailored energy levels, virtue of optimization of materials processing parameters and new fabrication methodologies. OSCs can be made flexible, semitransparent and are light weight, which offer an attractive option for achieving low-cost and clean energy sources. The unique flexibility and semi-transparency feature also add a decorative and aesthetic dimension to OSCs so that they can be used on curved and irregular surfaces, which cannot be done using traditional rigid silicon solar cells. The ubiquitous adoption of OSC technology as one of the primary energy sources will reduce greenhouse gas emissions, thus contributing to the preservation of our environment.

References

1. Ginley D S, Green M A, Collins R T. Solar energy conversion toward 1 terawatt. Mrs Bulletin, 2008, 33(4): 355–364
2. Slaoui A, Collins R T. Advanced inorganic materials for photovoltaics. Mrs Bulletin, 2007, 32(3): 211–218
3. Tang C W, VanSlyke S A. Organic electroluminescent diodes. Applied Physics Letters, 1987, 51(12): 913–915
4. Burroughs J H, Bradley D D C, Brown A R, Marks R N, MacKay K, Friend R H, Burn P L, Holmes A B. Light-emitting diodes based on conjugated polymers. Nature, 1990, 347(6293): 593–541
5. Li Y Q, Tan L W, Hao X T, Ong K S, Zhu F R, Hung L S. Flexible top-emitting electroluminescent devices on polyethylene terephthalate substrates. Applied Physics Letters, 2005, 86(15): 153508-1–153508-3
6. Bao Z A, Dodabalapur A, Lovinger A J. Soluble and processable regioregular poly(3-hexylthiophene) for thin film field-effect transistor applications with high mobility. Applied Physics Letters, 1996, 69(26): 4108–4110
7. Moller S, Perlov C, Jackson W, Taussig C, Forrest S R. A polymer/semiconductor write-once read-many-times memory. Nature, 2003, 426(6963): 166–169
8. Peumans P, Yakimov A, Forrest S R. Small molecular weight organic thin-film photodetectors and solar cells. Journal of Applied Physics, 2003, 93(7): 3693–3723
9. Tang C W. Two-layer organic photovoltaic cell. Applied Physics Letters, 1986, 48(2): 183–185
10. Shah A, Torres P, Tscharner R, Wyrsch N, Keppner H. Photovoltaic technology: the case for thin-film solar cells. Science, 1999, 285 (5428): 692–698
11. Yu G, Gao J, Wudl F, Heeger A J. Polymer photovoltaic cells: enhanced efficiencies via a network of internal donor-acceptor heterojunctions. Science, 1995, 270(5243): 1789–1791
12. Halls J J M, Walsh C A, Greenham N C, Friend R H, Holmes A B. Efficient photodiodes from interpenetrating polymer networks. Nature, 1995, 376(6540): 498–500
13. Tsuzuki T, Shirota Y, Meissner D. The effect of fullerene doping on photoelectric conversion using titanyl phthalocyanine and a perylene pigment. Solar Energy Materials and Solar Cells, 2000,

61(1): 1–8
14. Zhang F, Svensson M, Inganas O. Soluble polythiophenes with pendant fullerene groups as double cable materials for photodiodes. Advanced Materials, 2001, 13(24): 1871–1874
15. Kietzke T, Neher D, Landfester K, Montenegro R, Güntner R, Scherf U. Novel approaches to polymer blends based on polymer nanoparticles. Nature Materials, 2003, 2(6): 408–412
16. Marks R N, Halls J J M, Bradley D D C, Friend R H, Holmes A B. The photovoltaic response in poly(p-phenylene vinylene) thin-film devices. Journal of Physics Condensed Matter, 1994, 6(7): 1379–1394
17. Barth S, Bässler H, Rost H, Hörhold H H. Intrinsic photoconduction in PPV-type conjugated polymers. Physical Review Letters, 1997, 79(22): 4445–4448
18. Miranda P B, Moses D, Heeger A J. Ultrafast photogeneration of charged polarons in conjugated polymers. Physical Review B: Condensed Matter and Materials Physics, 2001, 64(8): 81201-1–81201-4
19. Brabec C J, Zerza G, Cerullo G, De Silvestri S, Luzzati S, Hummele J C, Sariciftci N S. Tracing photoinduced electron transfer process in conjugated polymer/fullerene bulk heterojunctions in real time. Chemical Physics Letters, 2001, 340(3–4): 232–236
20. Orenstein J. In: Skotheim T J, ed. Handbook on Conducting Polymers, Vol 2, p1297; or Kuzmany H, Mehring M, Roth S, eds. Springer Series in Solid State Sciences 76, Electronic Properties of Conjugated Polymers
21. Vardeny Z, Tauc J. Method for direct determination of the effective correlation energy of defects in semiconductors: optical modulation spectroscopy of dangling bonds. Physical Review Letters, 1985, 54 (16): 1844–1847
22. Vardeny Z, Ehrenfreund E, Brafman O, Nowak M, Schaffer H, Heeger A J, Wudl F. Photogeneration of confined soliton pairs (bipolarons) in polythiophene. Physical Review Letters, 1986, 56 (6): 671–674
23. Österbacka R, An C P, Jiang X M, Vardeny Z V. Two-dimensional electronic excitations in self-assembled conjugated polymer nanocrystals. Science, 2000, 287(5454): 839–842
24. Jiang X M, Österbacka R, Korovyanko O, An C P, Horovitz B, Janssen R A J, Vardeny Z V. Spectroscopic studies of photoexcitations in regioregular and regiorandom polythiophene films. Advanced Functional Materials, 2002, 12(9): 587–597
25. De S, Pascher T, Maiti M, Jespersen K G, Kesti T, Zhang F, Inganäs O, Yartsev A, Sundström V. Geminate charge recombination in alternating polyfluorene copolymer/fullerene blends. Journal of the American Chemical Society, 2007, 129(27): 8466–8472
26. Brabec C J, Zerza G, Cerullo G, De Silvestri S, Luzzati S, Hummelen J C, Sariciftci S. Tracing photoinduced electron transfer process in conjugated polymer/fullerene bulk heterojunctions in real time. Chemical Physics Letters, 2001, 340(3-4): 232–236
27. Clarke T, Ballantyne A, Jamieson F, Brabec C, Nelson J, Durrant J. Transient absorption spectroscopy of charge photogeneration yields and lifetimes in a low bandgap polymer/fullerene film. Chemical Communications (Cambridge), 2009, 1(1): 89–91
28. Hwang I W, Moses D, Heeger A J. Photoinduced carrier generation in P3HT/PCBM bulk heterojunction materials. Journal of Physical Chemistry C, 2008, 112(11): 4350–4354
29. Hwang I W, Soci C, Moses D, Zhu Z, Waller D, Gaudiana R, Brabex C J, Heeger A J. Ultrafast electron transfer and decay dynamics in a small band gap bulk heterojunction material. Advanced Materials, 2007, 19(17): 2307–2312
30. Clarke T M, Ballantyne A M, Nelson J, Bradley D D C, Durrant J. Free energy control of charge photogeneration in polythiophene/fullerene solar cells: the influence of thermal annealing on P3HT/PCBM blends. Advanced Functional Materials, 2008, 18(24): 4029–4035
31. Saricifci N S, Smilowitz L, Heeger A J, Wudi F. Photoinduced electron transfer from a conducting polymer to buckminsterfullerene. Science, 1994, 258(5087): 1474–1476
32. Peet J, Kim J Y, Coates N E, Ma W L, Moses D, Heeger A J, Bazan G C. Efficiency enhancement in low-bandgap polymer solar cells by processing with alkane dithiols. Nature Materials, 2007, 6(7): 497–500
33. Wang X Z, Tam H L, Yong K S, Chen Z K, Zhu F R. High performance optoelectronic device based on semitransparent organic photovoltaic cell integrated with organic light-emitting diode. Organic Electronics, 2011, 12(8): 1429–1433

Furong Zhu is a Professor in the Department of Physics and Associate Director of Institute of Advanced Materials (IAM) at Hong Kong Baptist University (HKBU). He received his B.Sc and M.Sc in Physics from Fudan University, Shanghai, China, in 1983 and 1987. He completed his Ph.D in Applied Physics at Charles Darwin University in Australia from 1990–1993. He did his post-doctoral research in the Department of Electrical and Electronic Engineering at Kyoto University in Japan from 1993–1995, and was a Research Fellow with the Department of Physics at Murdoch University in Australia from 1995–1997 working on silicon thin films derived from plasma enhanced chemical vapor deposition (PECVD) for device application. He joined Institute of Materials Research and Engineering (IMRE) in Singapore in 1997. Prior to HKBU, he was a Senior Scientist and a Program Manager leading the organic light-emitting diode (OLED) and organic photovoltaic (OPV) R&D activities at IMRE. He has authored/co-authored over 100 refereed journal/conference publications, and filed 8 patents in organic electronics. His research interests include device physics, surface science, nanostructures and semiconducting materials-oriented research for application in OLEDs, OPV, thin film transistors and organic sensors. He has been invited to deliver more than 30 invited talks at the different international conferences.